2013

# An Extended Flux Model-Based Rotor Position Estimator for Sensorless Control of Interior Permanent Magnet Synchronous Machines

Yue Zhao
*University of Nebraska-Lincoln*, yue.zhao@huskers.unl.edu

Zhe Zhang
*University of Nebraska-Lincoln*

Wei Qiao
*University of Nebraska-Lincoln*, wqiao@engr.unl.edu

Long Wu
*John Deere Electronic Solutions*, WuLong@JohnDeere.com

Energy Conversion Congress and Exposition (ECCE), 2013 IEEE
Year: 2013
Pages: 3799 - 3806, DOI: 10.1109/ECCE.2013.6647204

# An Extended Flux Model-Based Rotor Position Estimator for Sensorless Control of Interior Permanent Magnet Synchronous Machines

Yue Zhao and Zhe Zhang
Power & Energy Systems Laboratory
Department of Electrical Engineering
University of Nebraska-Lincoln
Lincoln, NE 68588-0511 USA
yue.zhao@huskers.unl.edu

Wei Qiao
Power & Energy Systems Laboratory
Department of Electrical Engineering
University of Nebraska-Lincoln
Lincoln, NE 68588-0511 USA
wqiao@engr.unl.edu

Long Wu
John Deere Electronic Solutions
4101 19th Avenue North
Fargo, ND 58102 USA
WuLong@JohnDeere.com

***Abstract*—Starting from the classical dynamic model of interior permanent magnet synchronous machines (IPMSMs) expressed in the stationary reference frame, this paper presents a mathematical model reconstruction process for IPMSMs, from which an extended flux-based IPMSM model is derived. Compared with the commonly used extended electromotive force-based model, the extended flux-based model has notable advantages of simpler model structure and less sensitive to machine parameter and speed variations. An extended flux model-based position estimator is then proposed for sensorless control of an IPMSM by utilizing a sliding-mode observer with a dynamic position compensator. The latter improves the dynamic performance and low-speed operating capability of the sensorless controller. Both simulation and experimental results are provided to validate the proposed position estimator and sensorless IPMSM drive system.**

***Index Terms*—Extended flux model; position estimation; interior permanent magnet synchronous machine (IPMSM); sensorless control**

## I. INTRODUCTION

In recent years, much research effort has gone into the development of position/speed sensorless drives that have comparable dynamic performance with respect to the sensor-based drives for IPMSMs [1]-[7]. In the medium- and high-speed range, the electromotive force (EMF)-based method is one of the most widely used strategies for rotor position estimation [1]-[3]. However, in the low-speed region, due to the small signal-to-noise ratio (SNR), i.e., the ratio between the magnitude of the EMF and the magnitude of noise, the EMF-based position estimators are not accurate enough. Thus, the capability of the EMF-based position estimators should be further improved for low-speed operations.

Due to machine rotor saliency, the position estimation algorithm for an IPMSM is generally more complex than that for a nonsalient permanent magnet synchronous machine (PMSM), e.g., a surface-mounted PMSM. To perform the EMF-based position estimation for IPMSMs, several reconstructed EMF- or flux-based IPMSM models have been proposed. The "extended EMF (EEMF)" model [1], [2] is the most widely used one, which can effectively convert the saliency-related voltage terms into the EMF terms, such that the reconstructed EEMF is a summation of the saliency-related EMF terms and the original back EMF terms. In the EEMF model, only the EEMF components contain the rotor position information. However, since the magnitude of the EEMF depends on the load and the change of the current, the dynamic performance of an EEMF-based position estimator may degrade during large load transients. Moreover, since the EEMF model needs the information of speed and machine parameters, i.e., stator resistance and inductances, it is difficult to design an observer which is robust to both load condition variations and machine parameter uncertainties. Besides the EEMF-based model, the models reconstructed based on the flux concept, e.g., the "fictitious flux" model [4] and "active flux" model [5], provide alternatives to convert an IPMSM model into an equivalent nonsalient PMSM model mathematically. In the flux model-based position estimation, an integrator is normally required to calculate the flux. In this case, some practical issues, e.g., integrator DC offset and initial condition, should be carefully handled.

This paper presents a mathematical model reconstruction process for dynamic modeling of IPMSMs. By reconstructing the IPMSM model using the voltage concept, the EEMF-based model can be obtained; by reconstructing the IPMSM model using the flux concept, a new extended flux-based IPMSM model can be derived. Compared to the EEMF model, the extended flux model has the advantages of simpler structure, independence to speed, and less sensitivity to machine parameter variations. Moreover, an extended flux model-based position estimator is proposed for sensorless control of IPMSMs by using an SMO with a dynamic position compensator. The latter is designed to improve the transient performance and low-speed operating capability of

This work was supported in part by the U.S. National Science Foundation under grant ECCS-0901218.

the sensorless drive. Extensive simulation results on a 3-hp IPMSM drive system and experimental results on a 50-kW IPMSM drive system are presented to validate the proposed position estimator and sensorless control.

## II. Model Reconstruction for IPMSMs

### A. Dynamic Model of an IPMSM

The dynamics of an IPMSM can be modeled in the $dq$ rotating reference frame as:

$$\begin{bmatrix} v_d \\ v_q \end{bmatrix} = \begin{bmatrix} R + pL_d & -\omega_{re}L_q \\ \omega_{re}L_d & R + pL_q \end{bmatrix} \begin{bmatrix} i_d \\ i_q \end{bmatrix} + \begin{bmatrix} 0 \\ \omega_{re}\lambda_m \end{bmatrix} \tag{1}$$

where $p$ is a derivative operator; $v_d$ and $v_q$ are the $d$-axis and $q$-axis stator voltages, respectively; $i_d$ and $i_q$ are the $d$-axis and $q$-axis stator currents, respectively; $\omega_{re}$ is the rotor electrical speed; $L_d$ and $L_q$ are the $d$-axis and $q$-axis inductances, respectively; $\lambda_m$ is the flux linkage produced by the permanent magnets, and $R$ is the stator resistance. Using the inverse Park transformation, the IPMSM model in the $\alpha\beta$ stationary reference frame can be expressed as:

$$\begin{aligned} \begin{bmatrix} v_\alpha \\ v_\beta \end{bmatrix} &= R\begin{bmatrix} i_\alpha \\ i_\beta \end{bmatrix} + p\begin{bmatrix} L + \Delta L\cos(2\theta_{re}) & \Delta L\sin\theta_{re} \\ \Delta L\sin\theta_{re} & L - \Delta L\cos(2\theta_{re}) \end{bmatrix}\begin{bmatrix} i_\alpha \\ i_\beta \end{bmatrix} \\ &\quad + \omega_{re}\lambda_m\begin{bmatrix} -\sin\theta_{re} \\ \cos\theta_{re} \end{bmatrix} \end{aligned} \tag{2}$$

where $L = (L_d + L_q)/2$, $\Delta L = (L_d - L_q)/2$, and $\theta_{re}$ is the rotor position angle. Due to the machine rotor saliency, i.e., $L_d \neq L_q$, both $\theta_{re}$ and $2\theta_{re}$ terms appear in (2). Therefore, it is difficult to use (2) directly for rotor position observation. To facilitate the rotor position observation, a reconstructed IPMSM model is needed.

This paper proposes to reconstruct the IPMSM model mathematically from a voltage/flux model as follows:

$$\begin{aligned} v_\alpha &= Ri_\alpha + \overbrace{L_d\,p\left(i_d\cos(\theta_{re})\right) - L_q\,p\left(i_q\sin(\theta_{re})\right) + \lambda_m p\left(\cos(\theta_{re})\right)}^{p\lambda_\alpha} \\ v_\beta &= Ri_\beta + \underbrace{L_d\,p\left(i_d\sin(\theta_{re})\right) + L_q\,p\left(i_q\cos(\theta_{re})\right) + \lambda_m p\left(\sin(\theta_{re})\right)}_{p\lambda_\beta} \end{aligned} \tag{3}$$

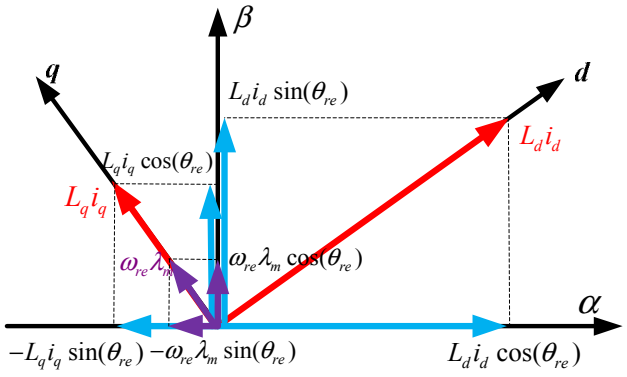


Fig. 1. Illustration of the IPMSM model (3).

Equation (3), which models the voltage/flux dynamics in the stationary reference frame, contains voltage terms ($v_\alpha$ and $v_\beta$) in the stationary reference frame and derivative of flux terms ($p\lambda_\alpha$ and $p\lambda_\beta$) in the rotating reference frame. In (3), only the $\theta_{re}$ related terms are present, and each term has clear physical meaning, as shown in Fig. 1. Rearranging (3), the following equations can be obtained:

$$\begin{aligned} \begin{bmatrix} v_\alpha \\ v_\beta \end{bmatrix} &= R\begin{bmatrix} i_\alpha \\ i_\beta \end{bmatrix} + p\begin{bmatrix} L & 0 \\ 0 & L \end{bmatrix}\begin{bmatrix} i_\alpha \\ i_\beta \end{bmatrix} \\ &\quad + \underbrace{\Delta L p\left(\begin{bmatrix} \cos\theta_{re} & \sin\theta_{re} \\ \sin\theta_{re} & -\cos\theta_{re} \end{bmatrix}\begin{bmatrix} i_d \\ i_q \end{bmatrix}\right) + \omega_{re}\lambda_m\begin{bmatrix} -\sin\theta_{re} \\ \cos\theta_{re} \end{bmatrix}}_{\text{Position Related Terms } V(\theta_{re})} \end{aligned} \tag{4}$$

### B. The Idea of Model Reconstruction

To facilitate position observation, the objective of model reconstruction for (3) is to achieve a similar symmetrical model structure as for the nonsalient PMSMs as follows.

$$\begin{aligned} \begin{bmatrix} v_\alpha \\ v_\beta \end{bmatrix} &= R\begin{bmatrix} i_\alpha \\ i_\beta \end{bmatrix} + p\begin{bmatrix} L_s & 0 \\ 0 & L_s \end{bmatrix}\begin{bmatrix} i_\alpha \\ i_\beta \end{bmatrix} + \omega_{re}\lambda_m\begin{bmatrix} -\sin\theta_{re} \\ \cos\theta_{re} \end{bmatrix} \\ &= R\begin{bmatrix} i_\alpha \\ i_\beta \end{bmatrix} + p\begin{bmatrix} L_s & 0 \\ 0 & L_s \end{bmatrix}\begin{bmatrix} i_\alpha \\ i_\beta \end{bmatrix} + p\begin{bmatrix} \lambda_m\cos\theta_{re} \\ \lambda_m\sin\theta_{re} \end{bmatrix} \end{aligned} \tag{5}$$

In (5), the $\sin(\theta_{re})$ and $\cos(\theta_{re})$ related terms are present separately in each equation. However, in (4), both the $\sin(\theta_{re})$ and $\cos(\theta_{re})$ related terms are present simultaneously in each equation. Therefore, further model reconstruction is required for (4) to achieve a similar model structure as (5). As shown in (5), the EMF term can be either written in the form of voltage, i.e., $\omega_{re}\lambda_m$ $[-\sin(\theta_{re})\ \ \cos(\theta_{re})]$, or in the form of derivative of flux, i.e., $p[\lambda_m\cos(\theta_{re})\ \lambda_m\sin(\theta_{re})]$. Similarly, (4) can be further reconstructed in either a voltage (EMF) or a flux form.

### C. Model Reconstruction Based on Voltage Concept

Considering the voltage form, the last two (position related) terms of (4) can be reconstructed as follows:

$$V(\theta_{re}) = \begin{bmatrix} \Delta L p\left(i_d\cos\theta_{re} + i_q\sin\theta_{re}\right) - \omega_{re}\lambda_m\sin\theta_{re} \\ \Delta L p\left(i_d\sin\theta_{re} - i_q\cos\theta_{re}\right) + \omega_{re}\lambda_m\cos\theta_{re} \end{bmatrix} \tag{6-1}$$

By using following inverse Park transform on currents

$$\begin{cases} i_\alpha = i_d\cos\theta_{re} - i_q\sin\theta_{re} \\ i_\beta = i_d\sin\theta_{re} + i_q\cos\theta_{re} \end{cases} \tag{6-2}$$

the following relationship can be obtained:

$$V(\theta_{re}) = \begin{bmatrix} \Delta L p\left(i_\alpha + 2i_q\sin\theta_{re}\right) - \omega_{re}\lambda_m\sin\theta_{re} \\ \Delta L p\left(i_\beta - 2i_q\cos\theta_{re}\right) + \omega_{re}\lambda_m\cos\theta_{re} \end{bmatrix} \tag{6-3}$$

In (6-3), the $\sin(\theta_{re})$ and $\cos(\theta_{re})$ related terms are present separately in each equation. However, both the voltage terms,

e.g., $\omega_{re}\lambda_m\sin(\theta_{re})$, and the derivatives of flux, e.g., $p(\Delta L i_q \sin(\theta_{re}))$, exist. $\sin(\theta_{re})$ and its derivative cannot be combined directly, neither $\cos(\theta_{re})$ and its derivative. Therefore, (6-3) needs further simplification. If the model reconstruction is based on voltage form, the derivatives of flux, e.g., $p(\Delta L i_q \sin(\theta_{re}))$, should be substituted by using pure voltage terms.

Applying (6-2) two more times in (6-3), the following equation can be obtained:

$$V(\theta_{re}) = \begin{bmatrix} \Delta L p(i_\alpha) + 2\omega_{re}\Delta L i_q \cos\theta_{re} - \left(\omega_{re}\lambda_m - 2\Delta L p(i_q)\right)\sin\theta_{re} \\ \Delta L p(i_\beta) + 2\omega_{re}\Delta L i_q \sin\theta_{re} + \left(\omega_{re}\lambda_m - 2\Delta L p(i_q)\right)\cos\theta_{re} \end{bmatrix} \quad (6-4)$$

$$= \begin{bmatrix} \Delta L p(i_\alpha) + 2\omega_{re}\Delta L i_\beta - \left[\omega_{re}(\lambda_m + 2\Delta L i_d) - 2\Delta L p(i_q)\right]\sin\theta_{re} \\ \Delta L p(i_\beta) - 2\omega_{re}\Delta L i_\alpha + \left[\omega_{re}(\lambda_m + 2\Delta L i_d) - 2\Delta L p(i_q)\right]\cos\theta_{re} \end{bmatrix}$$

Equation (6-4) is a part of the EEMF model proposed in [1]. The magnitude of the EEMF is denoted as $E_{ext}$ in this paper.

### D. Model Reconstruction Based on Flux Concept

Considering the flux form, the last two terms of (4) can be further reconstructed as follows:

$$V(\theta_{re}) = \Delta L p\left(\begin{bmatrix} \cos\theta_{re} & \sin\theta_{re} \\ \sin\theta_{re} & -\cos\theta_{re} \end{bmatrix}\begin{bmatrix} i_d \\ i_q \end{bmatrix}\right) + p\begin{bmatrix} \lambda_m \cos\theta_{re} \\ \lambda_m \sin\theta_{re} \end{bmatrix} = \begin{bmatrix} \Delta L p\left(i_d\cos\theta_{re} + i_q\sin\theta_{re}\right) + p\left(\lambda_m\cos\theta_{re}\right) \\ \Delta L p\left(i_d\sin\theta_{re} - i_q\cos\theta_{re}\right) + p\left(\lambda_m\sin\theta_{re}\right) \end{bmatrix} \quad (7-1)$$

By using (6-2), the following equation can be obtained:

$$V(\theta_{re}) = \begin{bmatrix} \Delta L p\left(2i_d\cos\theta_{re} - i_\alpha\right) + p\left(\lambda_m\cos\theta_{re}\right) \\ \Delta L p\left(2i_d\sin\theta_{re} - i_\beta\right) + p\left(\lambda_m\sin\theta_{re}\right) \end{bmatrix} \quad (7-2)$$

Different from (6-3), only the derivatives of flux, e.g., $p(\lambda_m\cos(\theta_{re}))$, are present in (7-2). Rearranging (7-2) yields

$$V(\theta_{re}) = \begin{bmatrix} -\Delta L p(i_\alpha) + p\left[\left(\lambda_m + 2\Delta L i_d\right)\cos\theta_{re}\right] \\ -\Delta L p(i_\beta) + p\left[\left(\lambda_m + 2\Delta L i_d\right)\sin\theta_{re}\right] \end{bmatrix} = \begin{bmatrix} -\Delta L p(i_\alpha) + p\left[\lambda_{ext}\cos\theta_{re}\right] \\ -\Delta L p(i_\beta) + p\left[\lambda_{ext}\sin\theta_{re}\right] \end{bmatrix} \quad (7-3)$$

The magnitude of the position related flux in (7-3) is defined as the extended flux and denoted as $\lambda_{ext}$, where $\lambda_{ext} = \lambda_m + 2\Delta L i_d$.

### E. Comparison of the Two Models

Substituting (6-4) and (7-3) into (4) yields the following EEMF model (8) proposed in [1] and the extended flux model (9), respectively.

$$\begin{bmatrix} v_\alpha \\ v_\beta \end{bmatrix} = \begin{bmatrix} R & \omega_{re}\left(L_d - L_q\right) \\ -\omega_{re}\left(L_d - L_q\right) & R \end{bmatrix}\cdot\begin{bmatrix} i_\alpha \\ i_\beta \end{bmatrix} + p\begin{bmatrix} L_d & 0 \\ 0 & L_d \end{bmatrix}\begin{bmatrix} i_\alpha \\ i_\beta \end{bmatrix} + E_{ext}\begin{bmatrix} -\sin\theta_{re} \\ \cos\theta_{re} \end{bmatrix} \quad (8)$$

where $E_{ext} = \omega_{re}\left[\lambda_m + \left(L_d - L_q\right)i_d\right] - \left(L_d - L_q\right)p\left(i_q\right)$.

$$\begin{bmatrix} v_\alpha \\ v_\beta \end{bmatrix} = \begin{bmatrix} R & 0 \\ 0 & R \end{bmatrix}\cdot\begin{bmatrix} i_\alpha \\ i_\beta \end{bmatrix} + p\begin{bmatrix} L_q & 0 \\ 0 & L_q \end{bmatrix}\begin{bmatrix} i_\alpha \\ i_\beta \end{bmatrix} + p\begin{bmatrix} \lambda_{ext}\cos\theta_{re} \\ \lambda_{ext}\sin\theta_{re} \end{bmatrix} \quad (9)$$

where $\lambda_{ext} = \lambda_m + \left(L_d - L_q\right)i_d$. A comparison between (8) and (9) is provided as follows:

*1)* A rotor position observer based on (8) needs the values of all machine parameters, including $R$, $L_d$ and $L_q$. However, a rotor position observer based on (9) does not need $L_d$ information.

*2)* In (8), $v_\alpha$ and $v_\beta$ are both functions of $i_\alpha$ and $i_\beta$. Therefore, the $\alpha$- and $\beta$-loops are not totally decoupled. However, in (9), $v_\alpha$ is a function of $i_\alpha$ only, and $v_\beta$ is a function of $i_\beta$ only. Therefore, the $\alpha$- and $\beta$-loops are decoupled.

*3)* In (8), the speed information, $\omega_{re}$, is needed; while (9) does not need $\omega_{re}$.

*4)* $E_{ext}$ in (8) depends on both $\omega_{re}$ and $p(i_q)$. Therefore, $E_{ext}$ is sensitive to load variations, which may degrade the dynamic performance of the observer. On the contrary, $\lambda_{ext}$ in (9) depends on neither $\omega_{re}$ nor $p(i_q)$. Therefore, an observer designed based on (9) should have better dynamic performance.

*5)* An observer can be designed based on (8) to obtain the EEMF directly, from which the rotor position can be easily estimated. However, an observer based on (9) can only be used to obtain the derivative of flux, and integration is needed to calculate the extended flux, from which the rotor position can be estimated.

In summary, an observer based on (9) is less sensitive to machine parameters, speed, and load variations than that based on (8). However, an integrator may be required to work with the observer together to calculate the extended flux, which can be used to extract the rotor position information directly.

## III. Sliding-Mode Observer with Dynamic Position Compensator for Rotor Position Estimation

To design an observer based on (9) without using an integrator, the most straightforward idea is to further process the derivative of the extended flux to obtain a voltage term that contains the rotor position explicitly. The derivative of

the extended flux can be viewed as a voltage term or EMF term, which is denoted as $e'_{\alpha\beta}$ and can be calculated as:

$$e'_{\alpha\beta}=\begin{bmatrix}e'_\alpha\\ e'_\beta\end{bmatrix}=p\begin{bmatrix}\lambda_{ext}\cos\theta_{re}\\ \lambda_{ext}\sin\theta_{re}\end{bmatrix}=\begin{bmatrix}\cos\theta_{re}\,p(\lambda_{ext})+\lambda_{ext}\,p(\cos\theta_{re})\\ \sin\theta_{re}\,p(\lambda_{ext})+\lambda_{ext}\,p(\sin\theta_{re})\end{bmatrix} \quad (10)$$
$$=\omega_{re}\lambda_{ext}\begin{bmatrix}-\sin\theta_{re}\\ \cos\theta_{re}\end{bmatrix}+(L_d-L_q)\,p(i_d)\begin{bmatrix}\cos\theta_{re}\\ \sin\theta_{re}\end{bmatrix}$$

As shown in (10), the $\cos\theta_{re}$ and $\sin\theta_{re}$ related terms are present simultaneously in the expressions of $e'_\alpha$ and $e'_\beta$. Therefore, it is still complex to estimate the rotor position using (10) directly. However, in some specific applications if $(L_d-L_q)\,p(i_d) \ll \omega_{re}\lambda_{ext}$ is satisfied, the last term in (10) can be ignored and the position estimation will be notably simplified [6]. However, this method has obvious limitation due to the assumption $(L_d-L_q)\,p(i_d) \ll \omega_{re}\lambda_{ext}$. To eliminate the limitation, $e'_{\alpha\beta}$ is processed as follows:

$$\begin{aligned}&e'_\alpha+je'_\beta\\ &=\omega_{re}\lambda_{ext}(-\sin\theta_{re}+j\cos\theta_{re})+p(\lambda_{ext})(\cos\theta_{re}+j\sin\theta_{re}) \quad (11)\\ &=p(\lambda_{ext})e^{j\theta_{re}}+j\omega_{re}\lambda_{ext}e^{j\theta_{re}}=Ae^{j(\theta_{re}+\varphi)}\end{aligned}$$

where:

$$A=\sqrt{(p(\lambda_{ext}))^2+(\omega_{re}\lambda_{ext})^2} \text{ and } \varphi=\tan^{-1}\left(\omega_{re}\lambda_{ext}/p(\lambda_{ext})\right).$$

If $p(\lambda_{ext})=0$, $|\varphi|$ will be equal to $\pi/2$, which means that the position calculated from $e'_{\alpha\beta}$,

$$\tilde{\theta}=\tan^{-1}\left[p(\lambda_{ext}\cos\theta_{re})/p(\lambda_{ext}\sin\theta_{re})\right],$$

is in quadrature with $d$-axis. However, in practical applications when the IPMSM operates in the low-speed region or has a large variation of the extended flux (e.g., caused by an abrupt $i_d$ change), $|\varphi|$ will not be exactly equal to $\pi/2$ and a phase error, $\Delta\theta=\text{sign}(\varphi)\cdot(\pi/2-|\varphi|)$, will exist.

This paper proposes to design an SMO based on the extended flux model (9) to estimate the extended flux components, from which $\tilde{\theta}$ can be obtained. Since $\tilde{\theta}$ is not an accurate estimation of the actual rotor position, a dynamic position compensator is further proposed to eliminate the error between $\tilde{\theta}$ and the actual position, such that the position estimation performance in low-speed operations and large load transients can be improved. The overall block diagram of the proposed position estimator is shown in Fig. 2, which contains three major parts: an SMO, an envelope detector, and a dynamic position compensator. To utilize digital controllers for IPMSM drives, a discrete-time SMO [9] is designed according to (9) as follows:

$$\begin{cases}\hat{i}_\alpha[k+1]=T_s\left(v^*_\alpha/L_q+lZ_\alpha[k]\right)+\left(1-T_sR/L_q\right)\hat{i}_\alpha[k]\\ \hat{i}_\beta[k+1]=T_s\left(v^*_\beta/L_q+lZ_\beta[k]\right)+\left(1-T_sR/L_q\right)\hat{i}_\beta[k]\end{cases} \quad (12)$$

where $T_s$ is the sampling period of the SMO; $v^*_\alpha$ and $v^*_\beta$ are the voltage commands generated by the current controllers; $Z_\alpha[k]$ and $Z_\beta[k]$ are the outputs of the switching function at the $k^{\text{th}}$ time step, which contain $e'_{\alpha\beta}$ components, if the sliding mode is enforced. The angle between the vector $e'_\alpha+je'_\beta$ and $\alpha$-axis can be estimated as: $\tilde{\theta}=\tan^{-1}(Z_\alpha/Z_\beta)$.

However, per previous discussion, $\tilde{\theta}$ needs to be compensated for the phase error to handle low-speed and transient conditions, and the compensated position $\Delta\theta$ can be calculated as follows:

$$\begin{aligned}\Delta\theta[k]&=sign(\varphi[k])\cdot\left(\frac{\pi}{2}-|\varphi[k]|\right)\\ \varphi[k]&=\tan^{-1}\left[\frac{\hat{\omega}_{re}[k]\hat{\lambda}_{ext}[k]T_s}{\hat{\lambda}_{ext}[k]-\hat{\lambda}_{ext}[k-1]}\right]\end{aligned} \quad (13)$$

where $\hat{\omega}_{re}$ and $\hat{\lambda}_{ext}$ are the estimated speed and extended flux, respectively. A dynamic position compensator, as shown in Fig. 2, is designed to obtain $\Delta\theta$ based on (13). The estimated position $\hat{\theta}$ is obtained by adding $\Delta\theta$ to $\tilde{\theta}$. The estimated speed $\hat{\omega}_{re}$ can then be obtained from $\hat{\theta}$ by using a moving average or phase-locked loop (PLL) method [10].

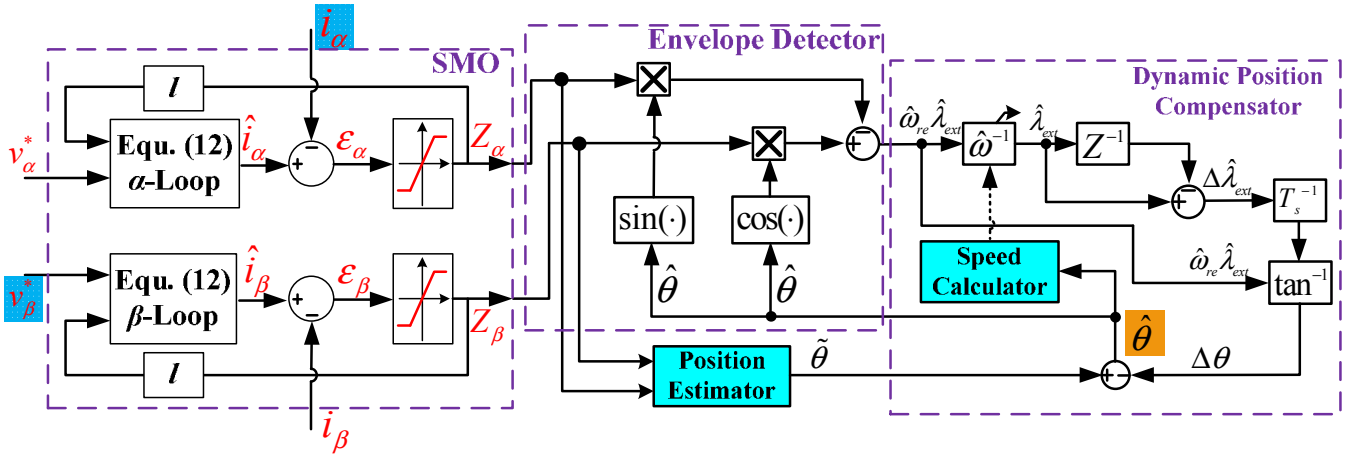


Fig. 2. Block diagram of the proposed position estimator.

An envelope detector is designed to estimate the product of $\hat{\omega}_{re}$ and $\hat{\lambda}_{ext}$ in (13), which can be expressed as:

$$Z_\beta \cos\hat{\theta} - Z_\alpha \sin\hat{\theta} \approx \hat{\omega}_{re}\hat{\lambda}_{ext} + p(\lambda_{ext})\sin(\theta_{re} - \hat{\theta}) \xrightarrow{\theta_{re} \approx \hat{\theta}} \approx \hat{\omega}_{re}\hat{\lambda}_{ext} \quad (14)$$

According to (14), if the error between the estimated and actual positions is small enough, the $\sin(\theta_{re} - \hat{\theta})$ term can be ignored, such that $\hat{\omega}_{re}\hat{\lambda}_{ext}$ is obtained. With the estimated speed, the magnitude of $\hat{\lambda}_{ext}$ can be further calculated.

## IV. Simulation Results

Per previous discussion, the proposed position estimator and sensorless drive system should have better dynamic performance and low-speed operating capability than the EEMF-based methods. In this section, simulation studies are performed to compare the performance of three different position estimators: the proposed position estimator, the proposed position estimator without the dynamic position compensator, and the EEMF-based position estimator proposed in [9], and the corresponding estimated positions are denoted as $\hat{\theta}_1$, $\hat{\theta}_2$, and $\hat{\theta}_3$, respectively. The parameters of the IPMSM used in the simulation are: $R$ = 3.1 Ω, $L_d$ = 38.6 mH, $L_q$ = 58.1 mH, $\lambda_m$ = 0.452 Vs/rad, rated power = 3 hp, rated speed = 1,250 RPM, rated torque = 12 Nm, and the number of pole pairs is 3. Some typical simulation results are shown in Figs. 3-6, including performance in torque control mode at 100%, 20% and 1% of the rated speed and in speed control mode.

Fig. 3 compares the performance of the three estimators when the IPMSM operates at the rated speed with different load variations. The commanded torque ($T^*$) and generated torque ($T_{em}$) of the system using the proposed position estimator are shown in Fig. 3(a). Both slow slew-rate and step-change torque reversals have been tested. The output torque of the sensorless drive system can well track the torque command. The position estimation errors obtained from the three estimators are compared in Fig. 3(b). The three position error profiles are on top of each other during slow slew-rate torque changes, which indicates that under this circumstance, the variation of the extended flux is quite small and can be ignored. Therefore, the performance of the three estimators is similar. However, when step torque changes are commanded, the position error is significantly reduced by using the proposed estimator, and the performance of the proposed estimator without the dynamic position compensator is still better than the EEMF-based position estimator. The profile of $\Delta\theta$ is shown in Fig. 3(c). It clearly shows when the torque changes with slow slew rates, $\Delta\theta$ is almost zero; however, when the torque experiences a step change, $\Delta\theta$ is a large value and cannot be ignored.

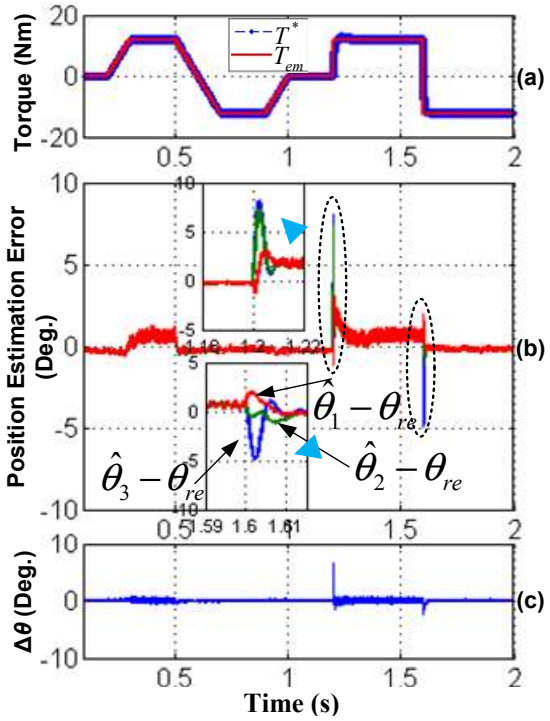


Fig. 3. Comparison of the three position estimators when the IPMSM operates at the rated speed with different load variations.

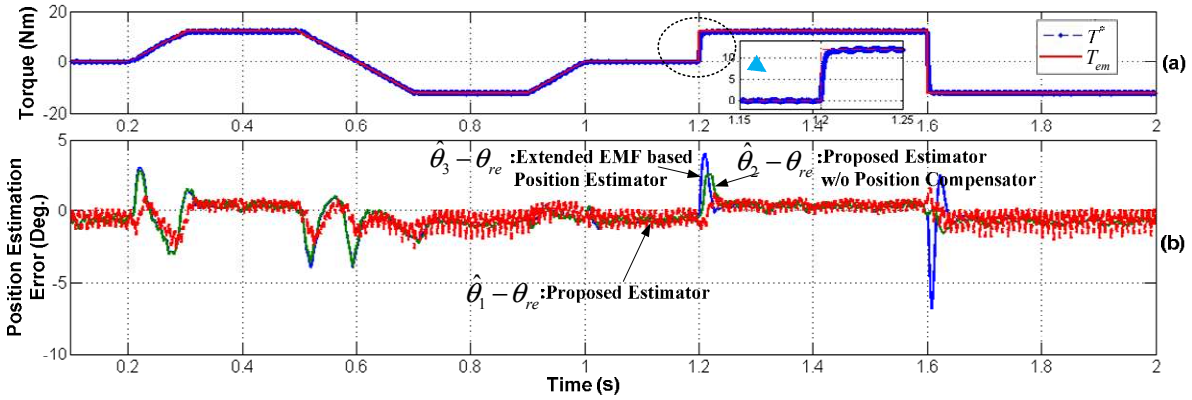


Fig. 4. Comparison of the three position estimators when the IPSMS operates at 20% rated speed with different load variations.

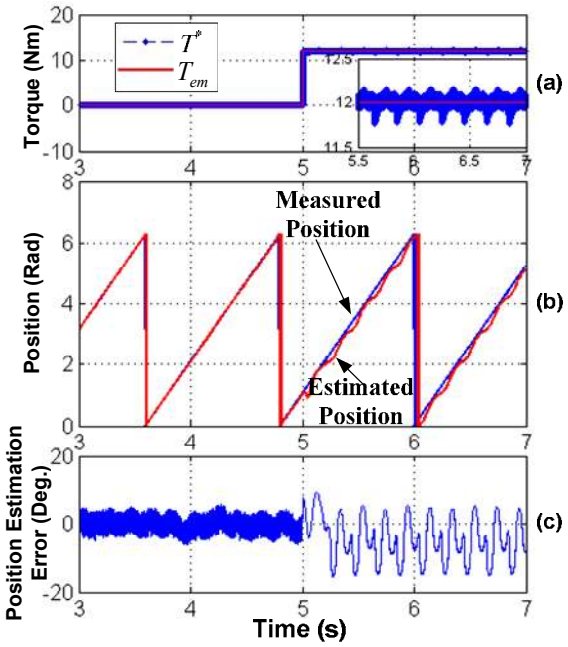


Fig. 5. Performance of the proposed position estimators when the IPMSM operates at 1% of rated speed under a step torque change.

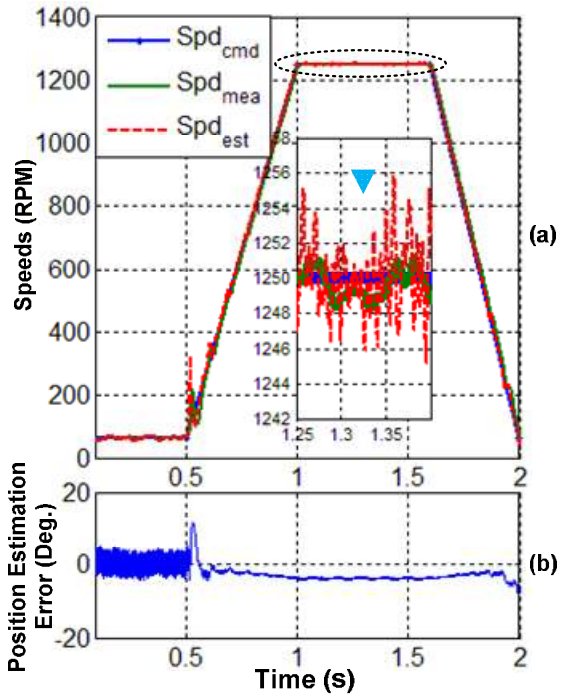


Fig. 6. Speed tracking performance of the sensorless drive using the proposed position estimator.

Fig. 4 compares the responses of the three estimators when the IPMSM operates at 20% of the rated speed, i.e., 250 RPM, with the same load variations as in Fig. 3. The transient performance of the proposed estimator is much better than the other two estimators. Fig. 5(a) shows the performance of the proposed estimator when the IPMSM operates at 1% of the rated speed, i.e., 12.5 RPM, during a step torque change. The EEMF-based position estimator and the proposed estimator without the position compensator both failed in this case. However, the proposed estimator still works and the accuracy of the position estimation is still acceptable, as shown in Fig. 5(b) and (c).

The speed response under no load condition of the sensorless drive equipped with the proposed position estimator is shown in Fig. 6. The profiles of the commanded speed ($Spd_{cmd}$), measured speed ($Spd_{mea}$) and estimated speed ($Spd_{est}$) are compared in Fig. 6(a). The machine speed increases from 5% of the rated speed, i.e., 62.5 RPM, to the rate speed within 0.5 s, stays at the rated speed for 0.6 s, and then decreases back to 62.5 RPM within 0.4 s. The sensorless control system shows good speed tracking performance during speed variations. The corresponding position estimation error, as shown in Fig. 6(b), is within ±4 electric degrees expect for an error spike at the beginning of the speed ramp-up, which however is settled down shortly.

## V. Experimental Results

Two different position estimators, i.e., the proposed position estimator and the EEMF-based position estimator proposed in [9], are implemented in the position/speed sensorless control software for an IPMSM test stand. In the experiments, the estimated position from one of these two position estimators is used as the control angle, and the other position estimator is disabled at that time. The test IPMSM has 5 magnetic pole pairs and the rated output power is 50 kW. The base speed is 2076 RPM and the maximum speed is 6500 RPM. The rated torque at the base speed is 230 Nm. The liquid-cooled inverter of the drive system is fed by a DC power supply, whose voltage is maintained at 700 V. The PWM switching frequency at the base speed is 2 kHz. The phase currents are sampled twice per PWM cycle, and the main control software (e.g., basic vector control, position estimation, etc.) implemented in the DSP interrupt service routine is also executed twice per PWM cycle.

To compare the transient performance of the two estimators, the results of ramp torque tests are shown in Figs. 7 and 8. In these tests, the IPMSM operates in the torque control mode, and its shaft speed is maintained at the based speed by a prime mover. In Fig. 7, the IPMSM is operated in the motoring mode and the torque command is ramped up from 0 Nm to 230 Nm. While in Fig. 8, a braking ramp torque is applied. As shown in the two figures, in both operating modes, the position estimation error of the proposed extended flux-based method has faster convergence speed and smaller oscillation. This indicates that the proposed method has better dynamic performance during torque transient compared to the EEMF-based method.

A more challenging case, complete torque reversal, is tested for the proposed sensorless control scheme. In this test, the operating mode of the IPMSM is reversed from full braking to full motoring, and the torque command is changed from −230 Nm to +230 Nm. In this test, long-time transient, torque zero-crossing, pulled-down DC bus voltage, could

cause trouble to the sensorless controller. The current tracking performance is shown in Fig. 9. During the torque transient, both $i_d$ and $i_q$ are well regulated.

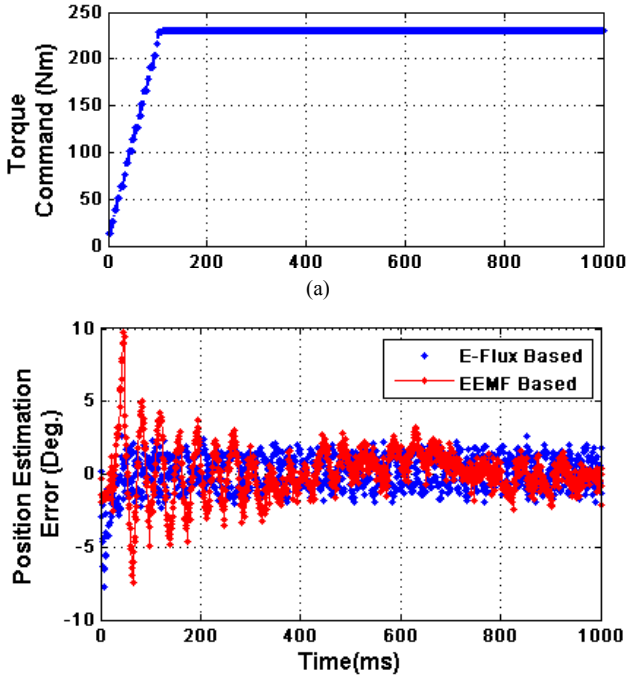


Fig. 7. Comparison of two position estimators during ramp (motoring) torque.

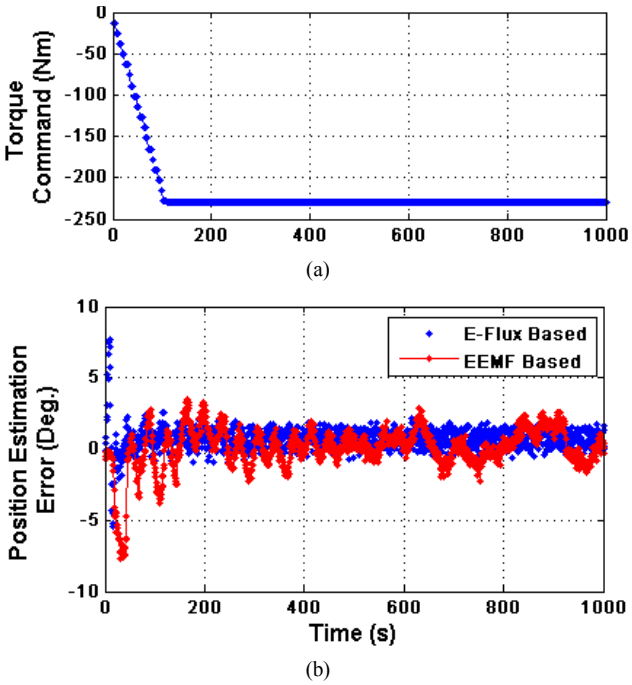


Fig. 8. Comparison of two position estimators during ramp (braking) torque.

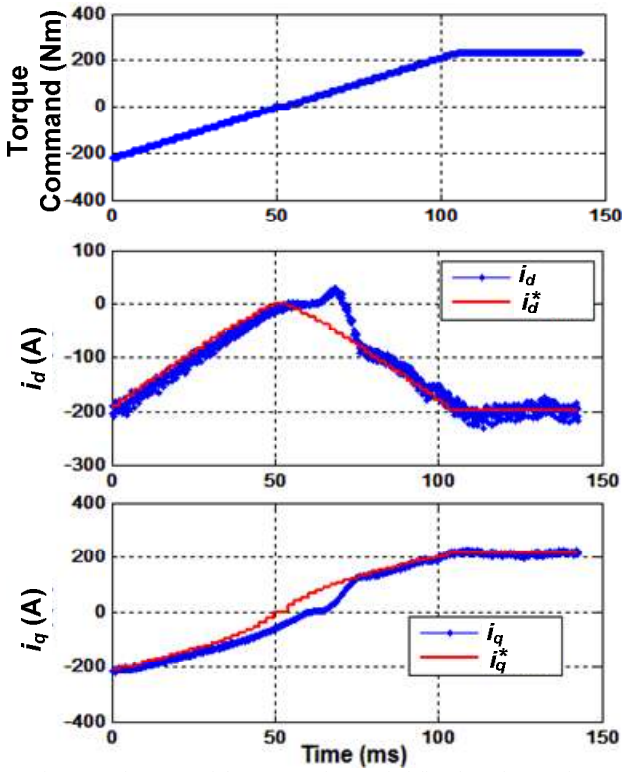


Fig. 9. Performnce of the proposed extended flux-based sensorless controller under complete torque reversal.

To verify the low speed operating capability, the proposed sensorless control scheme is tested at 5% of the base speed (2076RPM·5% = 103.8 RPM). As shown in Fig. 10(a), the rotor electric speed is maintained at 8.65 Hz. Due to the low speed and free shaft operation, the position error increased, when compared to the position error obtained at the rated speed. At this speed point, the position estimation error is limited within ±7 electric degrees. As shown in Fig. 10(a), the position estimation error has a speed dependent behavior. If the estimated speed is accurate, the position estimation error can be reduced by using a speed-based adjustment, e.g., a phase compensator. By zooming in the plots in Fig. 10(a), Fig. 10(b) shows the details of the results in three electric revolutions.

## VI. CONCLUSION

This paper has proposed a novel extended flux model-based position estimator for sensorless control of IPMSMs. The proposed extended flux model has notable advantages of simpler structure and improved robustness to the variations of machine parameters and load, when compared to the EEMF-based model. Extensive simulation results and experimental results have been provided to validate the proposed position estimator and sensorless control. Results have shown that, compared to the commonly used EEMF-based position estimator, the proposed estimator has much better dynamic performance and capability in very low-speed operating conditions.

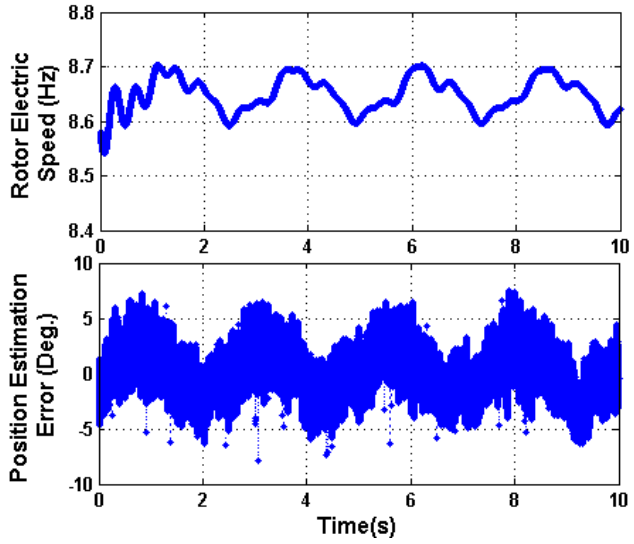


(a)

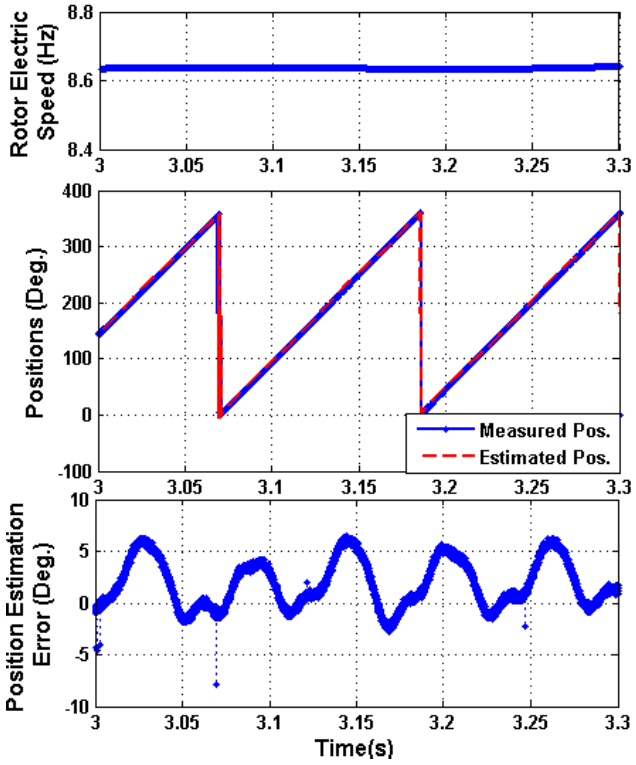


(b)

Fig. 10. Performnce of the proposed extended flux-based sensorless controller when the IPMSM opeates at 5% of the based speed.

## REFERENCES


[1] Z. Chen, M. Tomita, S. Doki, and S. Okuma, "An extended electromotive force model for sensorless control of interior permanent-magnet synchronous motors," *IEEE Trans. Industrial Electronics*, vol. 50, no. 3, pp. 288–295, Apr. 2003.

[2] S. Morimoto, K. Kawamoto, M. Sanada, and Y. Takeda, "Sensorless control strategy for salient-pole PMSM based on extended EMF in rotating reference frame," *IEEE Trans. Industrial Applications*, vol. 38, no. 4, pp. 1054-1061, Jul/Aug 2002.

[3] Y. Zhao, W. Qiao, and L. Wu, "An adaptive quasi-sliding-mode rotor position observer-based sensorless control for interior permanent magnet synchronous machines," *IEEE Trans. Power Electronics*, vol. 28, no. 12, pp. 5618-5629, Dec. 2013.

[4] S. Koonlaboon and S. Sangwongwanich, "Sensorless control of interior permanent-magnet synchronous motors based on a fictitious permanent magnet flux model," in *Proc. IEEE IAS Annual Meeting*, Oct. 2005, pp. 311–318.

[5] I. Boldea, M. C. Paicu, and G. D. Andreescu, "Active flux concept for motion sensorless unified ac drives," *IEEE Trans. Power Electronics*, vol. 23, no. 5, pp. 2612–2618, Sep. 2008.

[6] J. Liu, T. A. Nondahl, P. Schmidt, S. Royak, and M. Harbaugh, "Rotor position estimation for synchronous machines based on equivalent EMF," *IEEE Trans. Industry Applications*, vol. 47, no. 3, pp. 1310-1318, May-June 2011.

[7] G. Foo and M. F. Rahman, "Sensorless sliding-mode MTPA control of an IPM synchronous motor drive using a sliding-mode observer and HF signal injection," *IEEE Trans. Industrial Electronics*, vol. 57, no. 4, pp. 1270-1278, Apr 2010.

[8] Y. Zhao, W. Qiao and L. Wu, "Dead-time effect and current regulation quality analysis for a sliding-mode position observer-based sensorless IPMSM drives," in *Proc. IEEE IAS Annual Meeting*, Oct 2012, pp. 1-7.

[9] Y. Zhao, W. Qiao, and L. Wu, "Sensorless control for IPMSMs based on a multilayer discrete-time sliding-mode observer," in *Proc. IEEE Energy Conversion Congress and Exposition*, Sept. 2012, pp. 1788-1795.

[10] Y. Zhao, W. Qiao, and L. Wu, "Model reference adaptive system-based speed estimators for sensorless control of interior permanent magnet synchronous machines," in *Proc. IEEE Transportation Electrification Conference and Expo*, June 2013, pp. 1-8.